AIChE WILEY InterScience DISCOVER SOMETHING GREAT

ANN–Based Prediction of Two-Phase Gas–Liquid Flow Patterns in a Circular Conduit

H. Sharma, G. Das, and A. N. Samanta
Dept. of Chemical Engineering, Indian Institute of Technology, Kharagpur 721302, India

DOI 10.1002/aic.10922
Published online June 21, 2006 in Wiley InterScience (www.interscience.wiley.com).

The present study records an attempt to train artificial neural networks (ANNs) to develop an objective flow pattern indicator for air–water flows on the basis of the vast amount of data available in the literature. The technique should be capable of predicting the flow patterns as well as the intermediate bands of transition from known input variables such as the superficial velocity of the two phases, the pipe diameter, and its inclination. For this, the study tried three different types of ANN. The most commonly used feed-forward back-propagation (FFBP) technique accurately yields the flow patterns but fails when the transition regions are incorporated. The radial basis function network gives better predictions than those by FFBP but fails under certain flow conditions. The probabilistic neural network (PNN), based on Bayes–Parzen classification theory, gives accurate predictions of flow patterns for different pipe diameters and inclinations. It has been validated with both experimental and theoretical models available in the literature. It has next been used to generate generalized flow pattern maps for different pipe diameters and orientations. These maps reveal certain interesting features regarding the existence of flow patterns under different input conditions. PNN predicts the disappearance of the smooth stratified flow with slight inclinations from the horizontal orientation and the existence of churn flow only near the vertical orientation. © 2006 American Institute of Chemical Engineers *AIChE J,* 52: 3018–3028, 2006

Keywords: two-phase flow, artificial neural network (ANN), probabilistic neural network (PNN), flow pattern map, fluid mechanics, artificial intelligence

Introduction

During the simultaneous flow of two phases through any conduit, the two fluids can distribute themselves in a wide variety of ways that are not necessarily under the control of the experimenter or the designer. Depending on the intrinsic features and hydrodynamic parameters, the distribution can broadly be classified into different flow regimes or patterns. An accurate estimation of the different patterns is essential to the understanding and analysis of two-phase flow because not only the hydrodynamics but also heat- and mass-transfer characteristics depend on the phase distribution. Therefore, a large number of studies, both experimental and theoretical, have been reported with respect to characterization of the gas–liquid flow patterns.

Initial experiments[1] were based on the visual observations of the flow distributions under various fluid velocities, pipe diameters, and inclinations. Several objective methods (such as conductivity probe technique, radiation attenuation, and hot wire anemometry) were later adopted in combination with subjective judgments. These studies have often provided a subjective identification of the transition boundaries because the definitions of the patterns are primarily based on linguistic descriptions and graphical illustrations. Further, the proposed mechanistic models are based on an understanding of the physical mechanisms underlying the transitions. Because each transition is associated with a different mechanism, separate models are called for each of them. Moreover, because of the

Correspondence concerning this article should be addressed to G. Das at gargi@che.iitkgp.ernet.in.

© 2006 American Institute of Chemical Engineers

unknown physics of the flow situation, different researchers proposed different equations to predict the same transition and most of them are confined to air–water systems through a pipe of particular diameter and inclination. Barnea[2] attempted to develop a generalized map for the whole range of pipe inclinations, but could not provide an accurate estimation over certain ranges. Further, all the phenomenological models yielded single curves to demarcate the different patterns, whereas the patterns usually do not change abruptly under a fixed set of flow conditions. The transitions occur gradually over a range of flow rates during which one pattern degenerates to give way to a new distribution. For example, the small ripples at the interface during smooth stratified flow gradually give way to larger waves and the stratified wavy pattern sets in with increasing fluid velocities. The intermittent appearance of slug flow also does not occur in the whole pipe at the same time. There is a range of operating conditions during which some of the waves are large enough to intercept the continuity of the gas layer, whereas the stratified wavy appearance persists in the remaining portion of the pipe.

Considering the lacunae in the past literature and the importance of pattern characterization, the present work aims to develop an objective flow pattern indicator for gas–liquid systems. The indicator should be capable of predicting the regimes as well as the transition zones for air–water flow through a circular pipe of any orientation. It should be able to do so from easily measurable input parameters such as fluid velocities and physical properties, pipe diameter, and inclination. This calls for a nonlinear mapping from measurable physical parameters to flow regimes such that the mapping can be done without a detailed knowledge of the underlying process. The artificial neural network (ANN) appears to be a suitable tool for this purpose. Although it has not been used much in multiphase systems, a few fairly recent studies have demonstrated its enormous potential.

The earliest applications of neural networks to gas–liquid systems dates back to Cai et al.,[3] who adopted the Kohonen self-organizing feature map (KSOFM) model to classify the flow regimes during air–water two-phase horizontal flow from a set of pattern-sensitive stochastic features derived from absolute pressure signals. Tsoukalas et al.[4] adopted a neurofuzzy system to classify patterns during air–water upflow from the fluctuations of area-averaged void fractions and the probability density functions (PDFs) and power spectral densities (PSDs) of the impedance signal. Mi et al.[5,6] used signals from electrical capacitance probes as input to a neural network and identified flow patterns in a vertical channel with excellent results. They developed both supervised and self-organized neural network classifiers and noted that the self-organizing neural network self-discovered the information about flow-pattern transition. Gupta et al.[7] successfully applied a hybrid method based on four neural networks along with a simple first-principles model for prediction of the attachment rate constant in flotation columns. Yang et al.[8] demonstrated use of a neural network in the real-time determination of phase transport properties in high-pressure two-phase turbulent bubbly flows. They trained three back-propagation neural networks with the simulation results of a comprehensive theoretical model. Malayeri et al.[9] used the radial basis function network to predict the cross-sectional and the time-averaged void fractions at different temperatures during air–water two-phase upflow through vertical columns. They selected certain dimensionless groups—modified volumetric flow ratio, density difference ratio, and Weber number—as the input to the ANN. Xie et al.[10] examined the feasibility of a transportable ANN-based technique for the classification of flow patterns in three-phase gas–liquid–pulp fiber systems. They designed a three-layer feed-forward ANN that used seven inputs representing the characteristics of the spectral power density distribution of normalized pressure fluctuations. Some studies[11-13] also adopted ANN for modeling and control of fluidized beds.

The present study tried three types of ANN for identification of flow patterns and their underlying transitions. The most commonly used feed-forward back-propagation (FFBP) network could predict the flow patterns over the whole range of pipe inclinations but failed to provide an estimation of the transition bands. The radial basis network (RBN) gave better predictions than did the FFBP model but failed under certain transition conditions. Thus a probabilistic neural network (PNN) using radial basis function was adopted, which yielded generalized flow pattern maps with specified flow patterns and the intervening regions of transition zones from known parameters: superficial velocities, fluid properties, pipe diameter, and inclination. The trained network yielded flow patterns over the entire range of pipe inclinations at different conduit diameters and obtained certain interesting features about the occurrence of different flow patterns at different inclinations. The net predictions are in close agreement with the theoretical models reported in the literature for horizontal and vertical pipes. The slight mismatches in the maps were also present when the model equations were compared with experimental data generated by the authors themselves.

Collection of Data

The ANN was trained from the vast quantities of data available in the literature. Because it is a bad extrapolator but a good interpolator, large numbers of data over a wide range of phase flow rates were collected for a proper training and reasonably accurate prediction. The majority of the data reported in the literature are confined to air–water systems, and thus the ANN was trained for air–water systems only. The inputs required are the following:

(1) Air superficial velocity (U_{GS})
(2) Water superficial velocity(U_{LS})
(3) Pipe diameter (D)
(4) Pipe inclination (θ)

The data were collected in the different flow patterns as well as the transition between them. After a comprehensive survey of the past literature, the following flow pattern maps for the horizontal, vertical, and inclined pipes were used for generation of data:

(1) Mandhane et al.[1] map for horizontal pipes of 1-in. diameter.

(2) Taitel et al.[14] maps for vertical pipes of diameters 2.5 and 5.1 cm, whereas superficial gas and liquid velocities are the coordinates of the map.

(3) Weisman and Kang[15] maps for vertical and inclined pipes of diameters 2.5 and 5.1 cm at an inclination of 7° and 4.5 cm diameter at inclinations of 90 and 20.75°.

(4) Lin and Hanratty[16] map for horizontal pipes of 9.53 and 2.54 cm diameter.

(5) Barnea[2] flow pattern maps for air–water systems at 0.1 MPa, 25°C over the whole range of pipe inclinations (0, 1, 30, 80, and 90°) in a pipe of diameter 5.1 cm.

(6) Barnea et al.[17] flow regime maps for a 2.5 cm pipe at inclinations of 0.25, 2, and 10°.

The maps yielded a total of about 4000 data points. The only problem encountered in the compilation of data is the ambiguity in the definition and nomenclatures adopted by the different researchers to describe the patterns. Proper consistent definitions of the different patterns were thus adopted and a minimum number of patterns sufficient to describe the flow phenomena over a wide range of flow rates are identified in the present methodology.

Classification of Flow Patterns

The flow patterns have been classified according to the common character of the flow configurations where the common characters pertain to the distribution of the interface and the mechanisms dominating pressure drop and heat and mass transfer. Accordingly, the interfacial configurations reported for air–water flows through circular pipes have been classified by the present authors as dispersed bubbly, bubbly, plug, slug, churn, annular, smooth stratified, and wavy stratified flow patterns. The exercise yielded a total of 23 flow regimes for horizontal, vertical, and inclined flows. A schematic diagram of the different flow patterns thus defined (Figure 1) shows that the regimes encountered in horizontal flow are smooth stratified, wavy stratified, plug, dispersed bubbly, slug, and annular, whereas those observed in vertical pipes are bubbly, dispersed bubbly, slug, churn, and annular. Bubbly and dispersed bubbly are differentiated on the basis of bubble size and voidage profile. Dispersed bubbly flow consists of small spherical bubbles uniformly distributed in the geometry, whereas bubbly flow consists of a mixture of spherical and cap-shaped bubbles with a nonuniform voidage profile. This has also been referred to as the "churn turbulent bubbly flow" by many researchers. Plug flow consists of air plugs floating on the top of water in the horizontal flow (Figure 1), whereas slug flow has intermittent Taylor bubbles and aerated liquid slugs, occurring in both horizontal and vertical conduits. Smooth stratified and wavy stratified have been differentiated on the basis of interfacial characteristics.

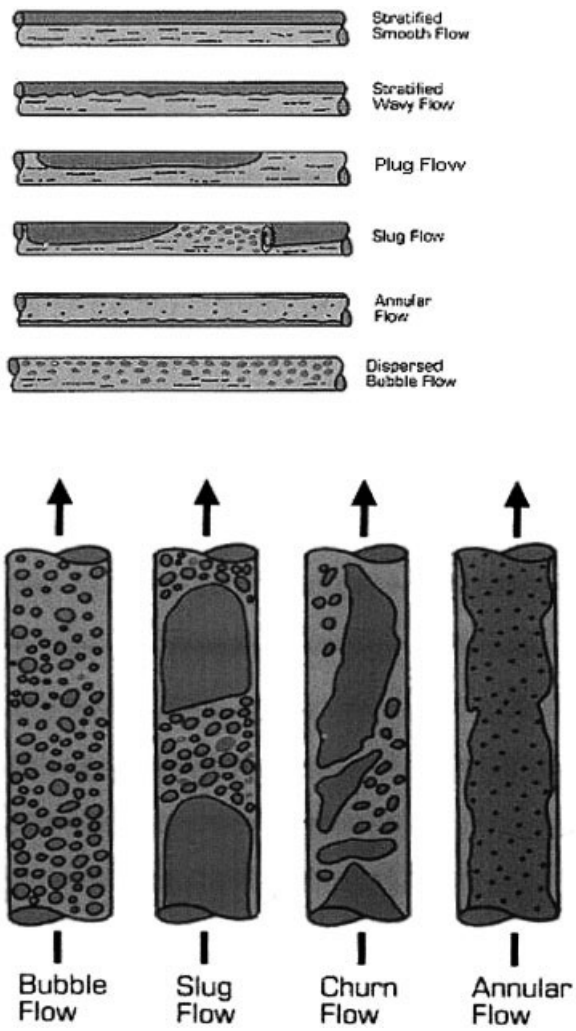

Figure 1. Different flow patterns in horizontal and vertical pipes.

The Neural Network Application

Three different types of artificial neural networks—back-propagation, radial basis functions, and probabilistic neural networks—have been used to generate models to predict flow patterns from operating and geometry data. Principles and theories of all these neural networks are well covered in the literature and are reviewed here only briefly. They are basically analytical tools that imitate the neural aspects of the human brain, whereby learning is based on experience and repetition rather than the application of rule-based principles and formulae. In essence, it can simply be viewed as a large dimensional regression model that can be used to correlate a vector X of input variables to a vector Y of output target variables, which can be approximated by a vector S by using the fitting parameters or connection weights obtained from the training algorithm. To ensure that the network has been properly trained, the learning process is performed in two phases: the training and the testing phases. Learning or training is equivalent to finding a surface in a multidimensional space that provides a best fit to the training data. Generalization is equivalent to the use of this multidimensional solution to interpolate data unseen by the network. The inputs and outputs are usually numeric values scaled between 0 and 1. To treat the output as a flow regime indicator, the flow regimes are treated like an ordinal variable having a natural ordering based on the observed typical sequence of regime transitions.

Feed-forward back-propagation network

This is one of the most widely used neural networks for pattern recognition and diagnostic systems. The past literature shows that almost all the researches in multiphase systems had adopted the FFBP network. The network in the present work consists of multiple input nodes, several hidden layers, and a single output where each neuron is connected to a large number of others. The input signal is passed among them and each of them calculates its own output (H_K) from the weights associated with connections using the equation

Table 1. Flow Patterns (without Transitions) and Their Numerical Values for FFBP Training

Flow Pattern	Numerical Value	Symbols Used in Figure 2
Plug flow	0	□
Bubble flow	1	•
Slug flow	2	○
Churn flow	3	×
Annular flow	4	+
Stratified flow	5	*

$$H_k = f(\Sigma\ w_{ik}I_i - \theta_k) \tag{1}$$

where $f(\cdot)$ is the sigmoidal transfer function, whereas w_{ik} and θ_k are the weight coupling the kth output node to the ith node of the input vector I and the associated bias for the kth output node.

Learning is achieved by the adjustment of the weights (w_{ik}) associated with the interneuron connections according to a modified gradient descent algorithm, expressed as

$$w_{ij}^m = w_{ij}^{m-1} - \alpha^m \frac{\partial E(w)}{\partial w_{ij}} + \beta^m(w_{ij}^{m-1} - w_{ij}^{m-2}) \tag{2}$$

which is designed to minimize the difference (E) between the actual and predicted output. Here m is an iteration counter and α^m is the learning weight. The second term represents the action of the error gradient that is back-propagated through the network. The last term is the momentum factor that forces the change of weight to proceed in the same direction as the previous change, thus speeding up the convergence of the algorithm and allowing the escape from narrow minima.

One of the main considerations in designing the network architecture is to decide the numbers of hidden layers and number of nodes in each hidden layer. Almost nothing has been mentioned in the literature and most of the past researchers worked with a single hidden layer. However, predictions from the FFBP network have been observed to improve significantly with inclusion of additional hidden layers. In the present work, an iterative technique has been adopted to determine the optimum ANN architecture. The change in root mean squared error (RMSE) on adding neurons to a particular layer is monitored and the optimum number of neurons in any layer yields the minimum RMSE for that layer. The RMSE is next estimated by adding a second hidden layer and the optimum neurons in this layer are determined as mentioned above. The architecture, which yields the minimum RMSE by this process, is thus selected. The ANN is checked against overtraining by noting the RMSE for the test data as well. The situation where the RMSE of the training data decreases, whereas that of the test data increases, with the number of iterations indicates an overtraining of the ANN. Thus both the number of iterations and

Table 2. RMSE for Both Training and Test Data for Different ANN Structures

Sample No.	Number of Hidden Layers	Nodes in Four Hidden Layers	Nodes in Three Hidden Layers	Nodes in Two Hidden Layers	Nodes in One Hidden Layer	RMSE for Training Data Set	RMSE for Test Data Set
1	1	0	0	0	1	0.112589	0.113624
2	1	0	0	0	2	0.110955	0.112617
3	1	0	0	0	3	0.100031	0.109011
4	1	0	0	0	4	0.099993	0.106475
5	1	0	0	0	5	0.096773	0.10798
6	1	0	0	0	6	0.090586	0.09825
7	1	0	0	0	7	0.080055	0.082878
8	1	0	0	0	8	0.080454	0.086489
9	1	0	0	0	9	0.10146	0.11209
10	1	0	0	0	10	0.084571	0.087734
11	1	0	0	0	11	0.076311	0.080859
12	1	0	0	0	12	0.089423	0.094711
13	1	0	0	0	13	0.098785	0.104561
14	2	0	0	1	11	0.095795	0.102137
15	2	0	0	2	11	0.087822	0.093606
16	2	0	0	3	11	0.080936	0.085333
17	2	0	0	4	11	0.070381	0.074603
18	2	0	0	5	11	0.05373	0.06011
19	2	0	0	6	11	0.078128	0.08319
20	2	0	0	7	11	0.074748	0.078227
21	2	0	0	8	11	0.076108	0.079248
22	2	0	0	9	11	0.062963	0.062731
23	3	0	1	5	11	0.108512	0.132154
24	3	0	2	5	11	0.073915	0.078341
25	**3**	**0**	**3**	**5**	**11**	**0.037949**	**0.047079**
26	3	0	4	5	11	0.059505	0.066283
27	3	0	5	5	11	0.059154	0.060831
28	3	0	6	5	11	0.074131	0.075133
29	4	1	3	5	11	0.108398	0.132449
30	4	2	3	5	11	0.077359	0.081912
31	4	3	3	5	11	0.111934	0.114137
32	4	4	3	5	11	0.073123	0.077769
33	4	5	3	5	11	0.122539	0.134359
34	4	6	3	5	11	0.126758	0.142176

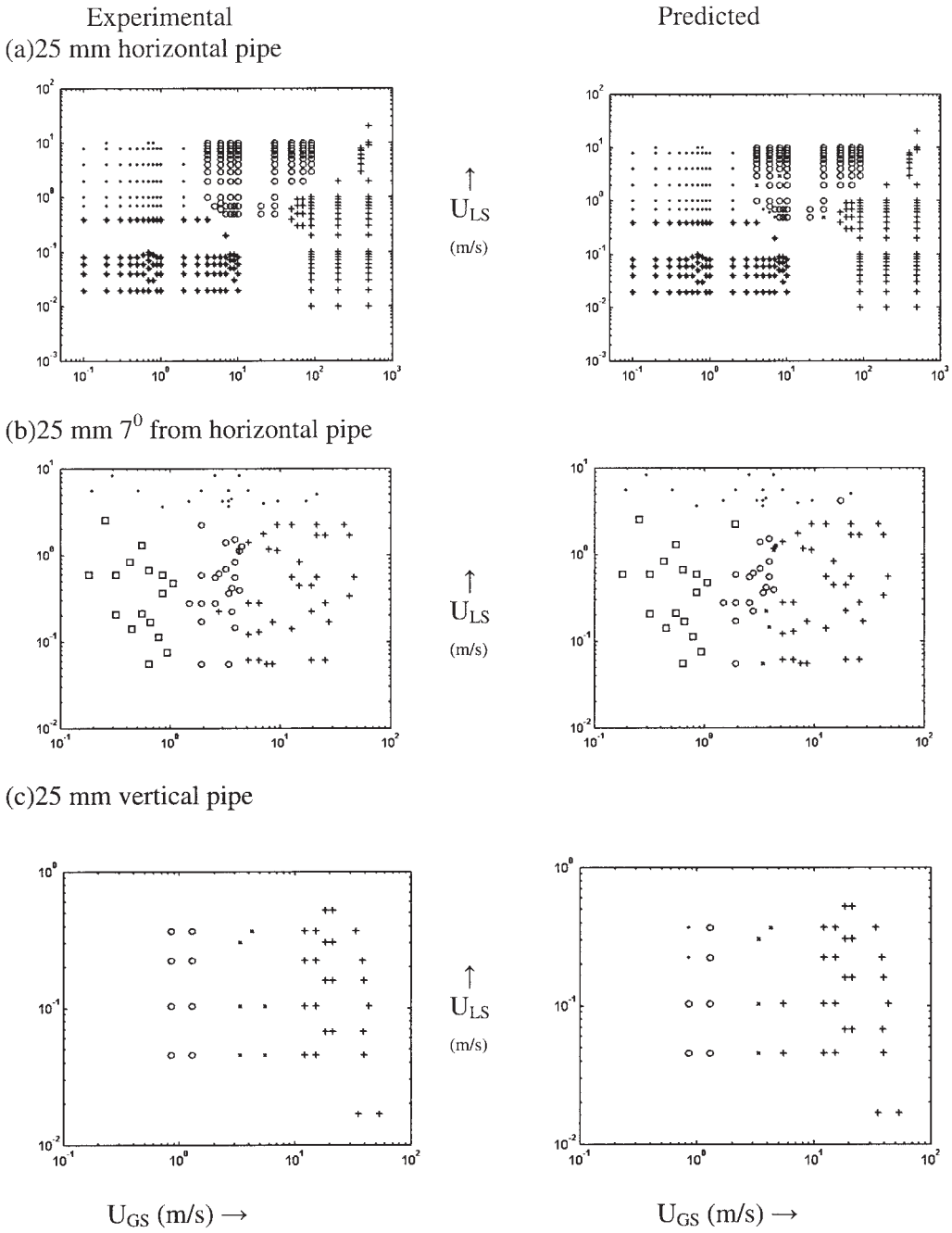

Figure 2. Experimental and predicted flow pattern maps for pipe flow.

the weights and bias are decided from a minimum in the RMSE of both the training and test data.

Training of FFBP for Identification of Flow Patterns. The FFBP in the present study is composed of four input nodes, U_{LS}, U_{GS}, D, and θ, and one output node, the flow pattern indicator. Before prediction of the pattern and the intervening transitions, the network is trained to estimate the fully developed flow patterns: plug, bubbly, slug, churn, annular, and stratified. They are numbered sequentially as shown in Table 1. A total of 2500 data were available in these flow regimes. Out of these 1500 data are used for training, whereas the remaining data are used as a test set.

The RMSEs of both the test and training data sets for increasing number of nodes in each hidden layer are reported in Table 2. The optimum architecture as obtained from the table (Sample No. 25, data in bold) constitutes three hidden layers with eleven, five, and three nodes in each of them. The addition of the fourth hidden layer increases the RMSE.

- *Results*: The flow regime maps as obtained from FFBP are validated against an experimental flow regime map for a 1-in. diameter pipe at inclinations of 0, 7, and 90 ° from the horizontal. The symbols used to denote the different flow patterns in the maps are listed in Table 1. There is a mismatch of six out of 314, three out of 38, and eight out of 91 data as shown in Figures 2a, 2b, and

Table 3. Flow Patterns (with Transitions) and Their Numerical Values for ANN Training

Sample No.	Flow Pattern	Numerical Value	Symbols in Figures 6–9
1	Dispersed bubbly flow	1	●
2	Bubbly flow	2	○
3	Plug flow	3	□
4	Slug flow	4	×
5	Annular flow	5	+
6	Wavy stratified flow	6	△
7	Smooth stratified flow	7	⊙
8	Smooth stratified—Wavy stratified	8	*
9	Smooth stratified—Bubbly	9	*
10	Wavy stratified—Annular	10	*
11	Wavy stratified—Slug	11	*
12	Slug—Annular	12	*
13	Plug—Annular	13	*
14	Plug—Slug	14	*
15	Dispersed bubbly—Annular	15	*
16	Dispersed bubbly—Plug	16	*
17	Dispersed bubbly—Slug	17	*
18	Dispersed bubbly—Bubbly	18	*
19	Bubbly—Slug	19	*
20	Churn—Annular	20	*
21	Churn—Slug	21	*
22	Churn—Dispersed bubbly	22	*
23	Churn flow	23	▷

2c, respectively. Values of standard deviation, maximum error, and correlation are 0.2440, 0.6, and 982, respectively.

Training of FFBP for Identification of Patterns and the Intervening Transitions. Attempts are next made to train the FFBP to predict both the flow patterns and the transitions between them, which has yielded a total of 23 patterns. The numbering of these patterns is listed in Table 3. A total of 4000 data are used for training and testing purposes. The optimum architecture is obtained from the plot of RMSE against the number of nodes in each hidden layer. The exercise showed that the ANN should consist of three hidden layers with 7, 8, and 11 nodes in each of them. This yielded an RMSE of 0.0431 for the training data and 0.0659 for the test data.

- *Results*: Predictions of the FFBP thus designed are compared with the experimental data to judge its suitability as a pattern identifier. Figure 3 shows the large number of mismatches and brings out the failure of FFBP when transition zones are considered. This can be attributed to the large amount of input data and the increased range of outputs in this case. Moreover, the closeness between the transitions and the flow regimes makes it difficult for the FFBP to distinguish between the two.

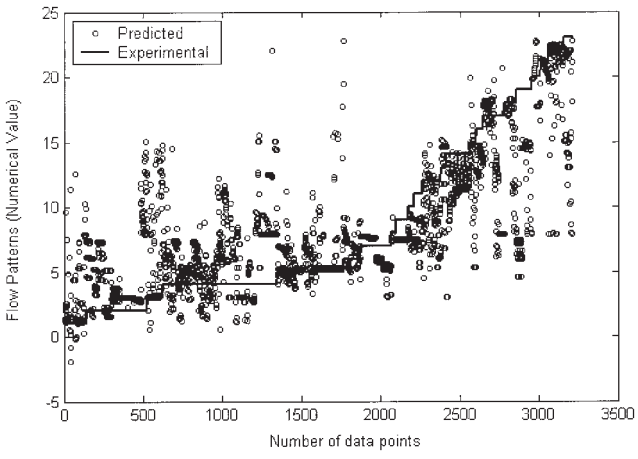

Figure 3. Comparison between experimental data and predictions of FFBP when transitions are considered.

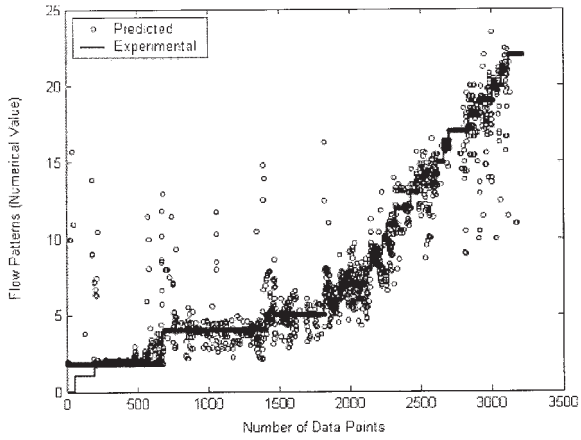

Figure 4. Comparison between experimental data and predictions of RBFN.

- Accordingly an alternative technique—the radial basis function network—was tried for a better clustering of data in a flow regime and a proper differentiation between them.

Radial basis function network (RBFN)

Although there are several similarities between the RBF and FFBP networks, it proves to be a potential alternative for FFBP because of its better approximation property and speed of convergence. It has been found to possess excellent nonlinear function approximation and generalization capabilities.[18,19] However, it has not been exploited to a significant extent for application to multiphase flow modeling. The only work was reported by Malayeri et al.,[9] who adopted this strategy to estimate the void fraction of air–water two-phase flow system at elevated temperatures.

In its most basic form, the RBFN involves three different layers: an input layer, a hidden (kernel) layer, and an output layer. The nodes or neurons within each layer are fully connected to the previous layer in a feed-forward architecture. The input variables are each assigned to a node in an input layer and pass directly to the only hidden layer without weights. The hidden layer consists of J locally tuned units and each unit has a radial basis function acting like a hidden node. The hidden node output $\Phi_j(x)$ calculates the closeness of the input and projects the distance to an activation function. The activation function of the jth hidden node used in this study is the Gaussian function given by

$$\Phi_j(x) = \exp\left(-\frac{\|x - \bar{x}_j\|^2}{2\sigma_j^2}\right) \tag{3}$$

where x is the n-dimensional input vector; $\bar{x}_j$ is the center of the radial basis functions for hidden node j; and $\|x - \bar{x}_j\|$ denotes

the Euclidean distance between the center of the radial basis function and input; and σ_j, the spread constant, is a parameter for controlling the smoothness properties of the radial basis functions. The third layer of the network is the output layer with L nodes that are fully interconnected to each hidden node. The output of the network is the sum of linear weighted $\Phi_j(x)$

$$y_1 = \sum_{j=0}^{J} w_{lj}\Phi_j(x) \tag{4}$$

where y_l is the lth component of the output layer; w_{lj} is the synaptic weight between the jth node of the hidden layer and the lth node of the output layer.

Training of RBFN to Predict Flow Patterns and Transitions. Training an RBFN for a specific problem involves selecting the type of basis functions with associated center location $\bar{x}_j$ and width or spread constant σ, the number of functions, and the

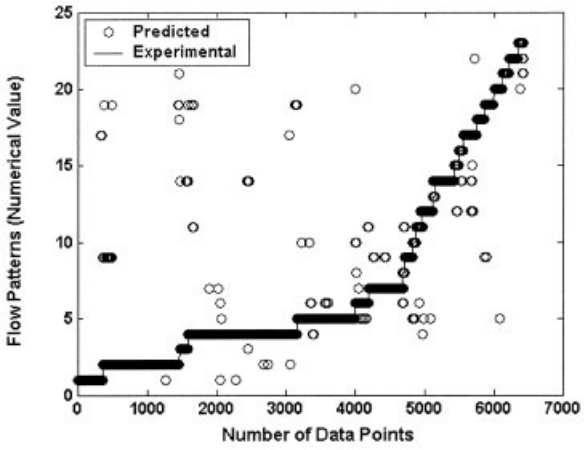

(a)

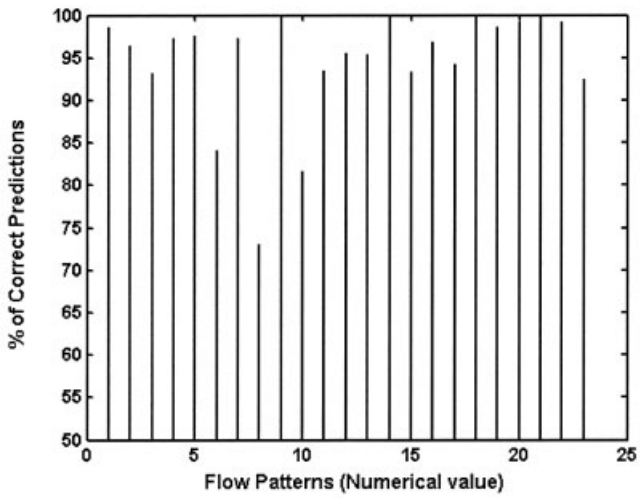

(b)

Figure 5. (a) Comparison between experimental data and predictions using PNN; (b) histogram depicting correctness in PNN prediction of flow patterns and their transitions.

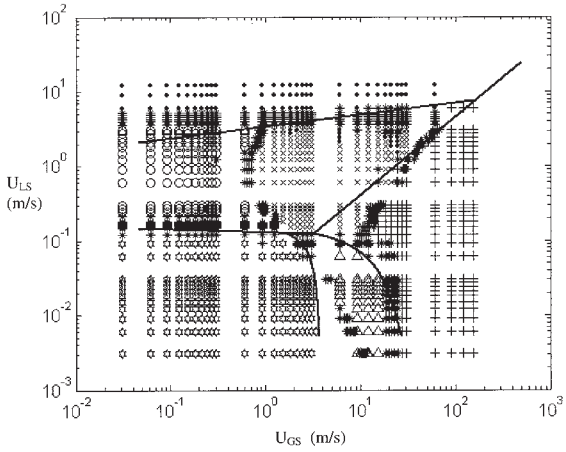

(a)

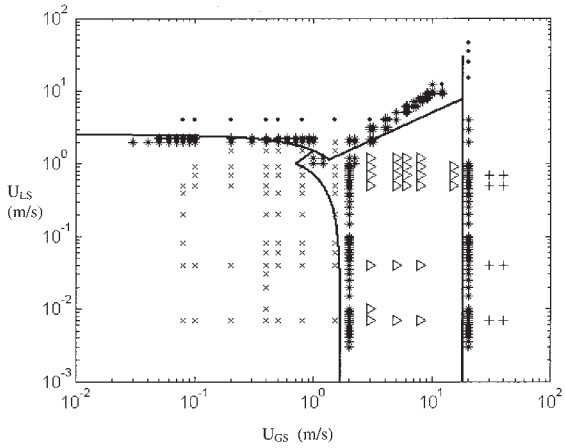

(b)

Figure 6. (a) Comparison of PNN predictions with the mechanistic models proposed by Taitel and Dukler[22] for a 1-in. horizontal pipe; (b) comparison of PNN predictions with the mechanistic models proposed by Taitel et al.[14] for a 1-in. vertical pipe.

weights. The RBF network is trained by a hybrid procedure that involves both unsupervised and supervised learning. In the first phase, the RBF layer is trained using the principle of self-organization (unsupervised learning), which primarily aims at positioning the centers for specified widths of the basis function. In the second phase, learning is implemented to evaluate the output layer weights. The present work adopted the rival penalizing competitive learning[20] for choosing the basis function centers and the singular value decomposition approach for estimating the weights of the output layer. This technique is advantageous because it automatically fixes the optimal number of basis functions, thereby avoiding the commonly used trial and error approach. In this technique, only one basis function is allotted to a single cluster and this is achieved by a penalizing mechanism where the center of the winning basis function is penalized using a much smaller learning rate than that used to update the winner.

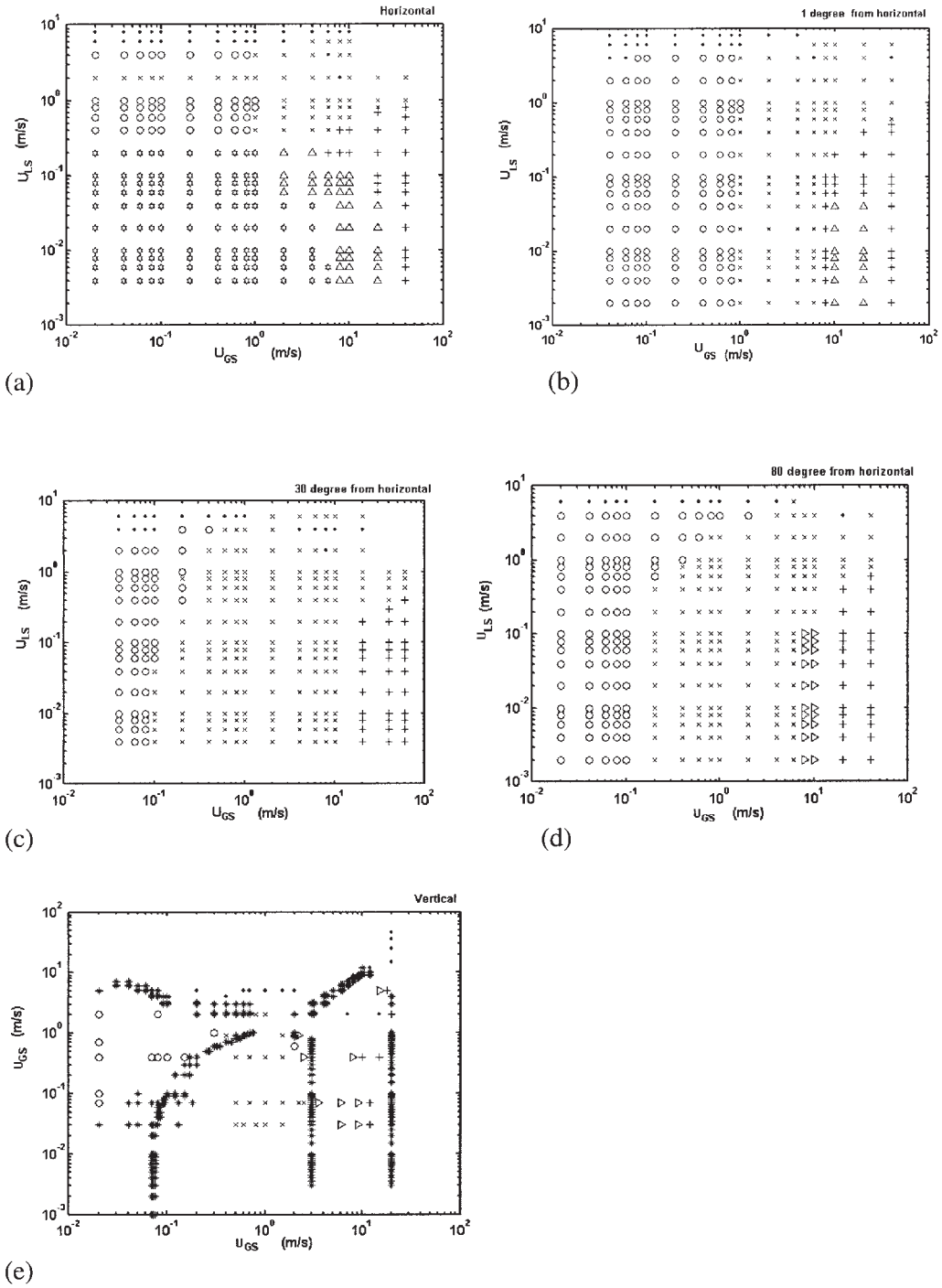

Figure 7. Effect of inclinations on flow patterns for 5.1 cm pipe.

The global minimum or a reasonable local minimum is estimated by performing a number of independent training runs by changing the spread constant of the radial basis functions. After each training session, the network's generalized performance is monitored using a test set consisting of representative input–output vectors, which are not part of the training set. The set of RBF centers, widths, and the output layer weights giving the least RMSE for the test is considered to be optimal.

- *Results*: In the present study, the RBFN was trained with various values of spread constant and a spread constant of 0.05 was observed to give the lowest RMSE. Figure 4 shows the validation of the predictions of RBFN with experimental data. The sequential numbering of the flow patterns and the symbols denoting each of them are itemized in Table 3. A comparison of Figure 4 with Figure 3 makes apparent the improvement in prediction of RBFN over that of FFBP.

- However, there are several mismatches in the figure that show there is scope for further improvement. Therefore, a better method—the PNN—was adopted next in this study.

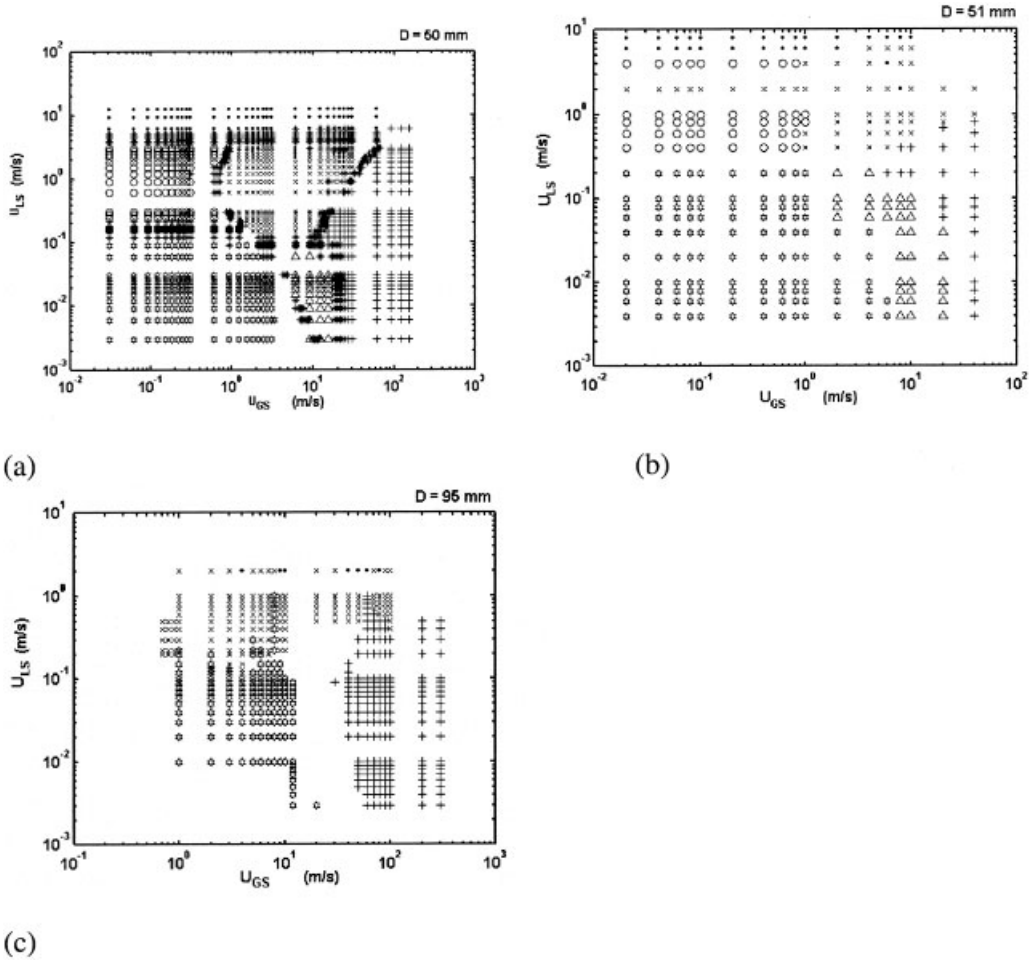

Figure 8. Effect of pipe diameter on flow patterns for horizontal flow.

The Probabilistic Neural Network

The probabilistic neural network (PNN) is based on the Bayes–Parzen classification theory. Specht[21] developed this kind of neural network and showed how the Bayes–Parzen classifier could be broken up into a large number of simple processes implemented in a multilayer neural network, each of which could be run independently in parallel. The architecture of a PNN is distinct from that of a standard back-propagation neural network and provides superior performance in classification applications. The PNN, which operates by defining a PDF for each data class based on the training set data and an optimized kernel width parameter (σ), consists of an input layer, a pattern layer, a summation layer, and an output layer. The pattern layer is designed to contain one neuron (node) for each training case available. At each neuron in the pattern layer, a distance measure is computed between the presented input vector and the training example represented by that pattern neuron and then processed through a Gaussian activation function as

$$\Phi_j(x) = \exp\left(\frac{\|x - \bar{x}_j\|^2}{2\sigma_j^2}\right) \tag{5}$$

where x is the vector of random variables and x_j is the jth training vector.

The summation layer sums the outputs from all hidden neurons of each respective data class. The results from the summation neurons are then compared and the largest is fed forward to the output neuron to yield the computed class and the probability that this example will belong to that class.

Training of PNN to Predict Flow Patterns and Transitions. The most important parameter that needs to be determined to obtain an optimal PNN is the spread constant (σ) of the random variables. The selection of this value is crucial because it determines the shape of the Gaussian functions. A large radius possesses a smooth shape and has the advantage of interpolation, and a small radius leads to a sharp shape and reduces the overlap between adjacent samples. However, too small a spread cannot generalize well because unknown samples lie only in the region in which Gaussian function enclosing can be generalized. A trial and error method was used to find the best radius. In the present work, the optimum spread constant (0.033) is calculated by minimizing the RMSE of the test set.

- *Results*: The PNN thus trained was used to generate flow pattern maps over the entire range of inclinations at different diameters and compared with both the experimental and the theoretical maps available in the literature.

Comparison of PNN Results with Experimental Flow Pattern Maps. The trained PNN is compared with 20 experimental flow pattern maps reported in the literature for horizontal,

vertical, and inclined pipes. Deviations of the experimental data from the training and test output are depicted in Figures 5a and 5b. A comparison of Figures 3 and 5a shows the improvement in prediction by PNN over that of FFBP. The histogram of Figure 5b further confirms the closeness with which PNN can estimate flow patterns and the intervening transitions over the entire range of pipe inclination. The figure shows that PNN provides an accurate prediction of flow patterns for >95% of the cases. The largest errors are observed at the transition between smooth and wavy stratified flows as well as stratified wavy and the annular flow patterns where the experimental identification is itself very difficult.

Comparison of PNN Results with Mechanistic Models. Attempts were next made to compare predictions of mechanistic models reported in the literature with those obtained from PNN. The most widely used model for horizontal pipes was proposed by Taitel and Dukler,[22] whereas that for vertical pipe was formulated by Taitel et al.[14] The model equations developed in these analyses to predict the different transitions were plotted in the flow pattern maps estimated from PNN for horizontal and vertical conduits, as shown in Figures 6a and 6b, respectively. The symbols used in the figures to depict the different flow patterns are listed in Table 2. The data in the transition bands are denoted by * for all cases. The model curves have been observed to be near or in the transition bands predicted by PNN. It may be mentioned that the slight mismatches evident from the figures are also present in the comparisons between the model and experimental predictions made by the authors themselves.

The Generalized Flow Pattern Map

The PNN has thus been observed to serve as an effective tool to identify the range of different flow patterns in existence at different inclinations and diameters of the conduit over the range of diameters used to train the PNN. Several flow pattern maps were generated using PNN under different input conditions. The superficial velocities of the liquid and gas phases were selected as the coordinate axes of the maps because the majority of the maps reported in the literature used the same data to graphically represent flow patterns. A few representative maps are presented in Figures 7–9. To understand the effect of inclination on the existence of different flow regimes, the flow pattern maps as predicted by PNN for a pipe of 5.1 cm diameter and different angles of inclination, ranging from a horizontal to a vertical orientation, are presented in Figure 7. The effect of pipe diameter is shown for both a horizontal and a vertical conduit in Figures 8 and 9, respectively, for three different diameters. A comparison of the different figures makes apparent certain interesting features:

- Smooth stratified flow occurs only for a horizontal pipe at an inclination of 0°. It has been observed to disappear even for very small inclinations. However, for increasing pipe diameters, this flow pattern exists over a larger range of flow velocities.
- On the other hand, the stratified wavy pattern exists for a longer range of inclination and its range of existence decreases with inclination, as expected, until it disappears completely. Moreover, as the pipe diameter is increased, this flow pattern exists for a smaller range of velocities.

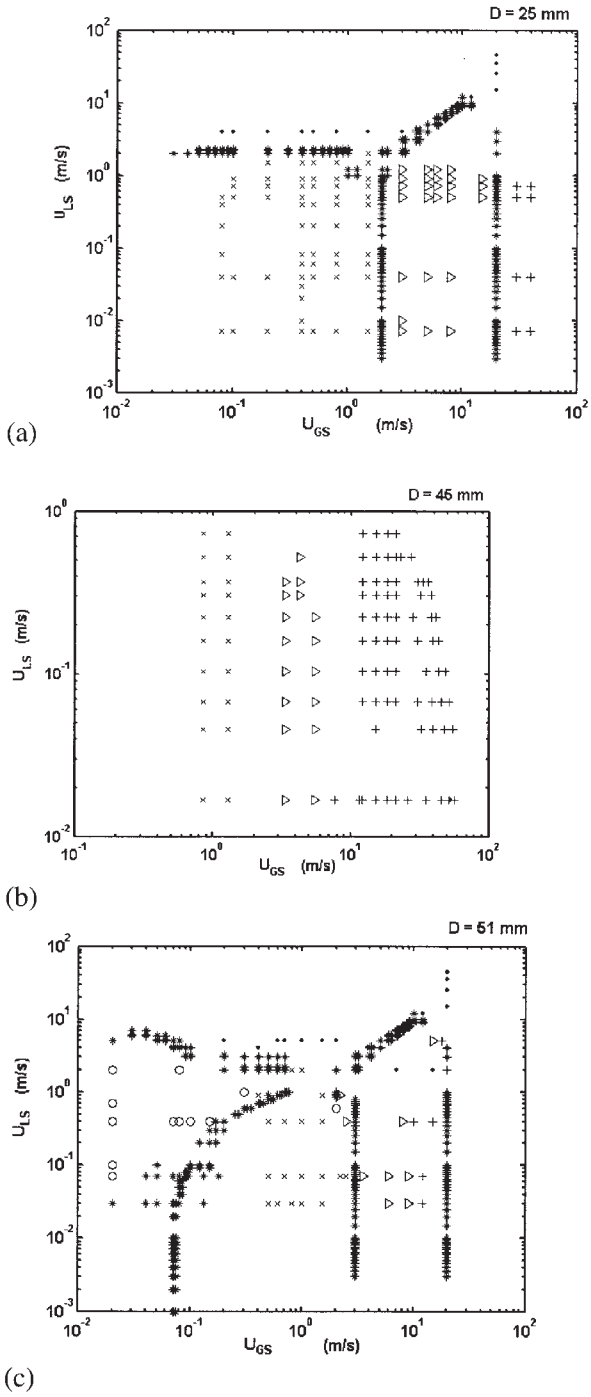

Figure 9. Effect of pipe diameter on flow patterns for vertical flow.

- Deviations from a horizontal orientation influence the flow patterns to a greater degree than do deviations from a vertical position.
- The churn flow pattern, which is absent in horizontal and slightly inclined pipes, sets in beyond an inclination of 80°.
- The slug flow pattern exists over a wide range of flow velocities in inclined and vertical pipes.
- Pipe diameter has a greater effect on flow patterns in the horizontal than that in the vertical orientation.

Conclusions

The present study adopted the artificial neural network to identify the flow patterns and the underlying bands of transition during air–water two-phase flow through circular pipes. It used easily measurable parameters—air superficial velocity (U_{GS}), water superficial velocity (U_{LS}), pipe diameter (D), and pipe inclination (θ)—as input to the network and obtained flow pattern as the output. It may be noted that the flow patterns were predicted from easily measurable parameters to make the predictions user friendly. However, certain other factors also influence the prevailing flow pattern. A few such factors include the wetting characteristics of the pipe, the design of the entry section, the influence of pipe contact angle with the fluid–fluid interface, and the variation of acceleration due to gravity. Nevertheless, the influence of pipe wall is felt mainly in capillaries and the other factors were not considered in the present work because data were not available.

For the training, the flow patterns were treated as ordinal variables having a natural ordering based on the observed typical sequence of pattern transitions. Three different neural networks were tried in this study. The most widely used feed-forward back-propagation network is observed to closely predict the flow patterns but fails to identify the transition regions. The radial basis function network, which gave a better prediction than that of the FFBP algorithm, fails under certain flow conditions. The probabilistic neural network (PNN) using radial basis function is observed to give the most accurate prediction of not only the range of different flow patterns but also the zones of transitions between them. The suitability of the PNN was validated with experimental flow pattern maps as well as model equations available in the literature. The PNN has been used as an objective flow pattern indicator for air–water flows through circular pipes at any inclination.

Literature Cited

1. Mandhane JM, Gregory GA, Aziz K. A flow pattern map for gas–liquid flow in horizontal pipes. *Int J Multiphase Flow.* 1974;1:537-553.
2. Barnea D. A unified model for predicting flow pattern transitions for the whole range of pipe inclinations. *Int J Multiphase Flow.* 1987;13:1-12.
3. Cai S, Toral H, Qiu J, Archer JS. Neural network based objective flow regime Identification in air–water two phase flow. *Can J Chem Eng.* 1994;72:440-445.
4. Tsoukalas LH, Ishii M, Mi Y. A neurofuzzy methodology for impedance-based multiphase flow identification. *Eng Appl Intell.* 1997;10:545-555.
5. Mi Y, Ishii M, Tsoukalas LH. Vertical two phase flow identification using advanced instrumentation and neural networks. *Nucl Eng Des.* 1998;184:409-420.
6. Mi Y, Ishii M, Tsoukalas LH. Flow regime identification methodology with neural networks and two-phase flow models. *Nucl Eng Des.* 2001;204:87-100.
7. Gupta S, Liu PH, Svoronos SA. Hybrid first-principles/neural networks model for column flotation. *AIChE J.* 1999;45:557-566.
8. Yang AS, Kuo TC, Ling PH. Application of neural network to prediction of phase transport characteristics in high-pressure two-phase turbulent bubbly flows. *Nucl Eng Des.* 2003;223:295-313.
9. Malayeri MR, Steinhagen HM, Smith JM. Neural network analysis of void fraction in air/water two-phase flows at elevated temperatures. *Chem Eng Process.* 2003;42:587-597.
10. Xie T, Ghiaasiaan SM, Karrila S. Artificial neural network approach for flow regime classification in gas–liquid–fiber flows based on frequency domain analysis of pressure signals. *Chem Eng Sci.* 2004;59:2241-2251.
11. Nakajima Y, Kikuchi R, Tsutsumi A, Otawara K. Nonlinear modeling of chaotic dynamics in a circulating fluidized bed by an artificial neural network. *J Chem Eng Jpn.* 2001;34:107-113.
12. Ottawara K, Fan LT, Tsutsumi A, Yashida K. An artificial neural network as a model for chaotic behavior of a three-phase fluidized bed. *Chaos Solitons Fractals.* 2002;13:353-362.
13. Chen W, Tsutsumi A, Lin H, Otawara K. Neural network approach to the prediction of nonlinear dynamics in a circulating fluidized bed. Proceedings of the 5th International Conference on Multiphase Flow, ICMF'04, Paper No. 127, Yokohama, Japan, May 30–June 4; 2004.
14. Taitel Y, Barnea D, Dukler AE. Modeling of flow pattern transition for steady upward gas–liquid flow in vertical tubes. *AIChE J.* 1980;26:345-353.
15. Weisman J, Kang SY. Flow pattern transition in vertical and upwardly inclined lines. *Int J Multiphase Flow.* 1981;7:271-291.
16. Lin PY, Hanratty TJ. Effect of pipe diameter on the flow patterns for air–water flow in horizontal pipes. *Int J Multiphase Flow.* 1987;13:549-563.
17. Barnea D, Shoham O, Taitel Y, Dukler AE. Flow pattern transition for gas–liquid flow in horizontal and inclined pipes: Comparison of experimental data with theory. *Int J Multiphase Flow.* 1980;6:217-225.
18. Broomhead DS, Lowe D. Multivariable functional interpolation and adaptive networks. *Complex Syst.* 1988;2:321-355.
19. Moody J, Darken C. Fast learning in networks of locally-tuned processing units. *Neural Comput.* 1989;1:281-294.
20. Xu L, Krzyzak A, Oja E. Rival penalized competitive learning for clustering analysis, RBF net and curve detection. *IEEE Trans Neural Netw.* 1993;4:636-649.
21. Specht DF. Probabilistic neural networks. *Neural Netw.* 1990;3:109-118.
22. Taitel Y, Dukler AE. A model for predicting flow regime transitions in horizontal and near horizontal gas–liquid flow. *AIChE J.* 1976;22:47-55.

Manuscript received July 18, 2005, and revision received May 12, 2006.